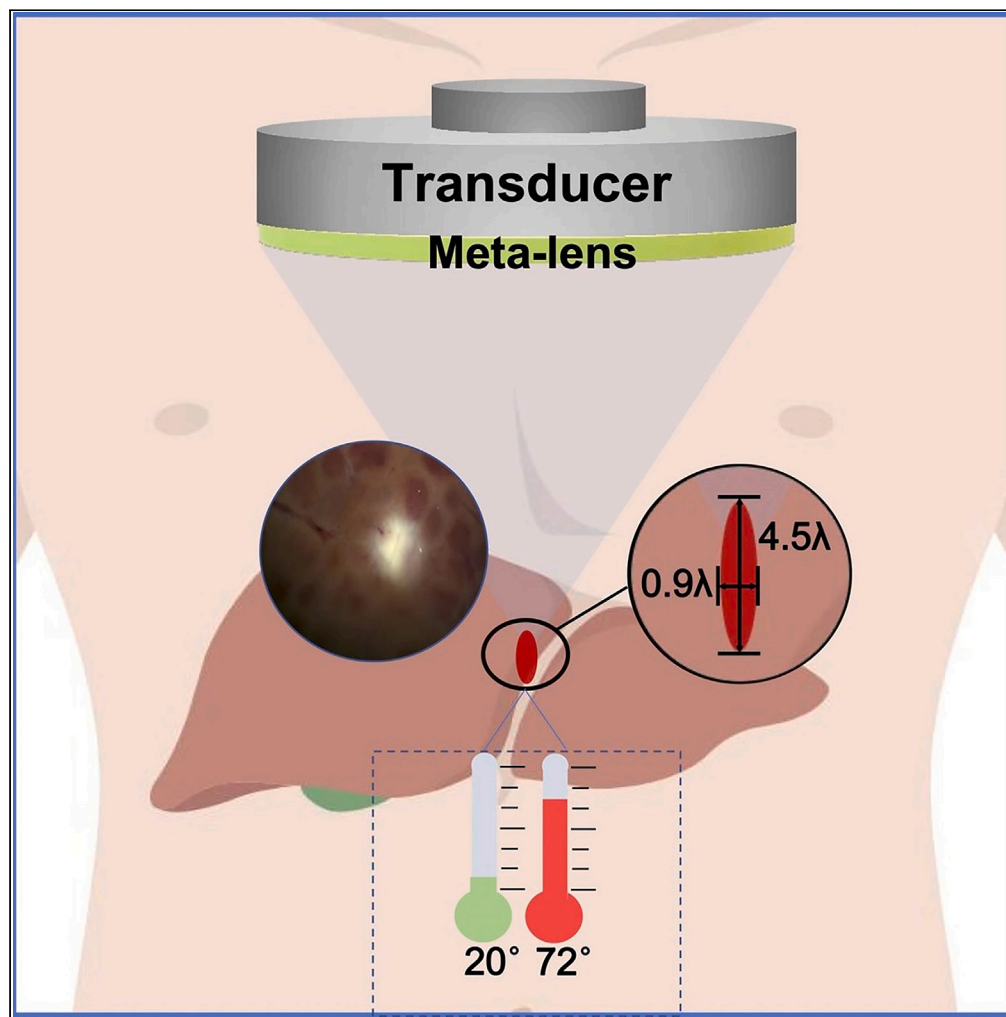


Article

Distinct thermal effect on biological tissues using subwavelength ultrasound metalens at megahertz



Yan Zheng, Chen Li, Chuanxin Zhang, Jiajie He, Xue Jiang, Dean Ta

xuejiang@fudan.edu.cn (X.J.)
tda@fudan.edu.cn (D.T.)

Highlights

The megahertz subwavelength ultrasonic metalens has high focusing resolution

Distinct thermal effect can be observed in biology phantom using metalens

Visible tissues lesions are induced at lower input power within a few seconds

Zheng et al., iScience 26, 107929
October 20, 2023 © 2023 The Author(s).
<https://doi.org/10.1016/j.isci.2023.107929>

Article

Distinct thermal effect on biological tissues using subwavelength ultrasound metalens at megahertz

Yan Zheng,¹ Chen Li,² Chuanxin Zhang,¹ Jiajie He,¹ Xue Jiang,^{1,5,*} and Dean Ta^{3,4,*}

SUMMARY

Ultrasound focusing plays an important role in biomedical therapy and diagnosis. Acoustic metalens has showcased remarkable focusing performance but yet to be implemented to the practical ultrasound therapeutic applications. We design a planar metalens operating at megahertz and experimentally demonstrate the distinct thermal effect on biological tissues induced by the high-resolution focusing. A prominent temperature rise of 50°C is experimentally observed in the biological phantom, with a much lower input ultrasound power of 4 W compared with the traditional methods. We further study the thermal effect on fresh porcine liver and investigate the morphological changes under different physical parameters. Visible lesions are observed in *in vitro* tissues at the lowest input ultrasound power of 2.6 W within 10 s. This study facilitates the practical biomedical application of acoustic metalens, providing a feasible approach for the precise, safe, and reliable therapeutic ultrasound with the simple and compact metalens.

INTRODUCTION

Therapeutic ultrasound has been applied in various clinical scenarios, such as tissue ablation,^{1–3} hemostasis,^{4–6} thrombolysis,^{7–10} cardiac pacing,^{11,12} therapeutic drug delivery,^{13–16} etc., bearing some unique characteristics including biocompatibility, superior penetrability, and nonionizing radiation.^{17–19} On this basis, focused ultrasound with the tightly converged energy distribution exhibits prominent advantage in improving the precision and safety of ultrasound treatment. Traditional ultrasound focusing methods are mainly relied on the active phased array or spherical transducer, which however cannot fulfill the requirements of high-precision, low-cost, and planar ultrasound therapy equipment. The active phased array can obtain the wavelength-scale resolution at the expense of complex and high-cost equipment,^{20,21} and the spherical transducer with curved bulky geometry fails to provide the sufficient focusing precision.^{22,23} A safer and more precise focused ultrasound technique with a simple configuration is highly required.

Rapid development of acoustic metamaterial/metasurface has made a significant breakthrough in sound-wave manipulation and provided new opportunities for higher-precision acoustic focusing with the passive and compact metalens.^{24–26} It is expected that the metalens-based focusing could provide promising potential in precision medical treatment, whereas several key technical issues should be figured out before the actual implementation. On the one hand, most of current researches on acoustic metamaterial/metasurface are restricted to airborne sound, which cannot be directly translated to the underwater ultrasound due to its shorter wavelength, stronger microstructural viscosity, and insufficient acoustic impedance contrast between the natural materials and water.²⁷ There are some attempts in designing ultrasound metalens, including the lens consisting of deep-subwavelength slots working around 100 kHz,²⁸ the Fresnel zone plate lens focusing ultrasound at 200 kHz,²⁹ the collimated ultrasound beam generated by the phononic crystal,³⁰ and the sparse metalens that reflects the ultrasound into a converged spot³¹ or an ultrasound scalpel.³² However, the transmission-type ultrasound metalens operating at megahertz is absent. On the other hand, investigation on thermal effect and morphological damage in biological tissues has yet to be demonstrated with the metalens-based ultrasound focusing. The positioning accuracy, focusing resolution, coupling efficiency, and energy transmittance are four critical factors affecting ultrasound focusing and further impacting therapeutic outcome. These factors remain to be improved in high-intensity focused ultrasound (HIFU) as well.^{33–35} Therefore, it is highly required to develop a new ultrasound therapeutic method with the millimeter-scale resolution, prominent temperature rise at low input energy, and precise damage in biological tissues.

In this work, we investigate the distinct thermal effect and morphological damage to *in vitro* biological tissues induced by the high-resolution ultrasound focusing based on metalens, which provides a novel ultrasound therapeutic method and plays as a feasible implementation of acoustic metalens in clinical applications. We theoretically design and experimentally realize the ultrasound metalens applicable to

¹Center for Biomedical Engineering, School of Information Science and Technology, Fudan University, Shanghai 200433, China

²Department of Ultrasound, Zhongshan Hospital, Fudan University, Shanghai 200032, P.R. China

³Center for Biomedical Engineering, School of Information Science and Technology, Fudan University, Shanghai 200433, China

⁴Department of Rehabilitation Medicine, Huashan Hospital, Fudan University, Shanghai 200040, China

⁵Lead contact

*Correspondence: xuejiang@fudan.edu.cn (X.J.), tda@fudan.edu.cn (D.T.)

<https://doi.org/10.1016/j.isci.2023.107929>



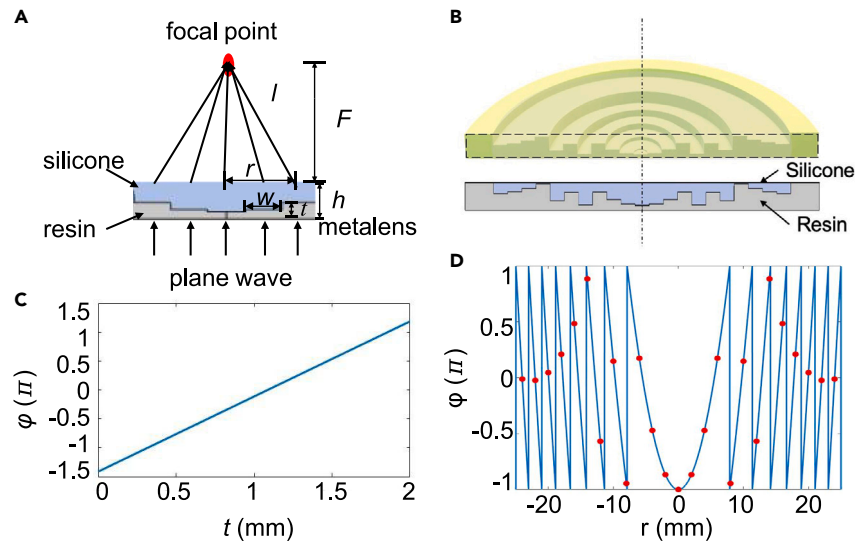


Figure 1. Schematic of ultrasound ablation on in vitro liver using metalens

(A) Schematic of the ultrasound manipulation principle with the metalens. The ultrasound emitted from every point on the metalens should arrive at the focal point in phase, which determines the initial phase profile on the metalens. The planar metalens with the overall thickness $h = 2$ mm is made of resin and silicone layers, whose thickness ratios are varied in radial direction to provide the required phase distribution. The continuous phase distribution in the radial is discretized and fulfilled by several concentric rings with the width $w = 2$ mm.

(B) Cross-section of the axisymmetric focusing lens with the diameter being 50 mm.

(C) Relationship between the phase shift and thickness of the resin layer in the metalens.

(D) Relationship between the required initial phase shift and radial position on the metalens for focusing at $F = 20$ mm. The discrete phase shifts achieved with the metalens of 11 concentric circular rings are denoted by the red dots.

work at megahertz, which can efficiently focus the transmitted ultrasound with the focusing resolution smaller than wavelength. The subwavelength focusing gives rise to the remarkable temperature rise of 50°C in the biological phantom, even with a much lower input ultrasound power of 4 W compared with the traditional methods. The thermal effect induced by the metalens-based focusing on the fresh vitro liver is further studied in experiments, and the morphological changes in the liver specimen under different parameter conditions are investigated, including quantification of the lesion area and lesion extent. Visible lesion is observed at the lowest input ultrasound power of 2.6 W owing to the high focusing resolution and energy efficiency of the metalens. In addition, the soft texture and planar geometry of the metalens guarantee the superior coupling with biological tissue and improve the biocompatibility of the metalens. The compact and passive metalens with the remarkable thermal effect would play as an ingenious way to overcome the aforementioned problems in ultrasound treatment and contribute to the integration and miniaturization of the functional devices in biomedical system.

RESULT

Theoretical model

Schematic diagram of ultrasound treatment on the vitro liver specimen with the metalens-based focusing is illustrated in Graphical Abstract, and the schematic of the ultrasound manipulation principle with the metalens is shown in Figure 1A. According to the Huygens principle, every point on the metalens is the source of spherical wavelets, the secondary wavelets emanating from different points mutually interfere, and the sum of these spherical wavelets forms a new wavefront. Therefore, the ultrasound emitted from every point on the metalens should arrive at the focal point in phase, which determines the initial phase profile $\varphi_1(r)$ on the metalens:

$$\varphi_1(r) + kl = \varphi_1(0) + kF + 2n\pi \quad (\text{Equation 1})$$

where $l = \sqrt{r^2 + F^2}$ is the propagation distance, F is the focal length, $k = 2\pi/\lambda$ is the wave number, and n is an arbitrary integer. The operating frequency in this work is 1 MHz ($\lambda = 1.5$ mm), which is a typically used value in ultrasound treatment. The initial phase at the center is set to be $\varphi_1(0) = 0$, and then the initial phase profile should satisfy

$$\varphi_1(r) = \frac{2\pi}{\lambda} \left(\sqrt{r^2 + F^2} - F \right) + 2n\pi \quad (\text{Equation 2})$$

The required phase profile with $F = 20$ mm is plotted in Figure 1D. The continuous phase profile is discretized with the interval of $w = 2$ mm in radial direction (denoted by the red dots) and fulfilled with a planar metalens. The ultrasound focusing metalens is consisted of concentric

Table 1. Acoustic parameters of different materials

Materials	Velocity (m/s)	Density (kg/m ³)
Water	1500	1000
Resin	2700	1180
Silicone	980	1264
Graphite phantom	1550	1045

circular rings that are constructed with the resin-silicon double layers, as shown in the cross-section of the metalens in Figure 1B. The overall thickness of the metalens is $h = 2$ mm, and the thickness ratios of each layer are controlled to provide the full-range ($0 \sim 2\pi$) phase manipulation of the transmitted wave. The phase shift of the transmitted ultrasound through the resin-silicone layers is as follows:

$$\varphi = \frac{2\pi}{\lambda}(h - h_{\text{eff}}) \quad (\text{Equation 3})$$

The effective acoustic path distance is as follows:

$$h_{\text{eff}} = \frac{c_r}{c_w}t + \frac{c_s}{c_w}(h - t) \quad (\text{Equation 4})$$

where t is the thickness of resin layer and c_r , c_s , and c_w are the sound speed in the resin, silicone and water, respectively. Measured material properties from experiments are shown in Table 1. Then the relationship between the required initial phase profile on the metalens and the resin thickness can be obtained, as plotted in Figure 1C. It is observed that the phase shift covering the full range from $-\pi$ to π is achieved by varying the thickness t from 0 to 2 mm. Finally, the metalens consisting of 11 concentric circular rings is designed, which fulfills the axisymmetric phase profile.

Subwavelength focusing with metalens

We carry out numerical simulations and experimental measurements to verify the focusing performance of the metalens (see STAR methods section). The normalized focused ultrasound intensity distribution on the axial plane ($z = 0$) obtained in simulation is demonstrated in Figure 2A. A typical ellipsoidal focal spot is observed at the position $z = 18.9$ mm, with a 5.5% deviation from the target focal length ($F = 20$ mm). Comparisons of the normalized ultrasound intensity fields between the simulations and experiments of the metalens and experiments of the concave lens on the focal plane (x - y plane, $z = 18.9$ mm) and axial plane (x - z plane, $y = 0$) are shown in Figure 2B. For better comparison, the ultrasound intensity is normalized with the corresponding maximum values in each situation throughout the paper. Good consistency is observed between the simulations and experiments, both of which verify the ultrasound focusing performance of the metalens. To quantitatively calculate the focal resolution, we plot the intensity profile along the axial (z) and transverse (x) directions through the focal spot, as shown in Figures 2C and 2D, respectively. The full width at half maxima (FWHM) and full length at half maxima (FLHM) of the focal point of the metalens in our experiment are 1.35 mm (0.9λ) and 6.75 mm (4.5λ), which clearly prove the subwavelength focusing performance of the metalens and contribute to the distinct thermal effect on biological tissue in the late study. The measured FWHM and FWLM of the concave lens are 1.8 mm (1.2λ) and 12.45 mm (8.3λ), respectively, which are much larger than the results with the metalens. In addition to the focusing resolution, the metalens bear the advantages of flat configuration to avoid the mismatch between the curved lens surface and planar tissue, and it also overcomes the restriction on the bound focal length and aperture. The planar metalens is beneficial to the integration with the flat transducer, which not only helps to improve the overall energy transmittance but also facilitates the development of more integrated and portable devices in the clinical ultrasound treatment. The soft texture of the metalens is skin-friendly and more suitable for clinical practice.

Temperature rising in biological phantom with ultrasound metalens

We then experimentally monitor the temperature rise during the metalens-based ultrasound focusing process in biological phantom. The biological phantom is made of an agar-based graphite material³⁶ whose acoustic properties (particularly, ultrasound speed and attenuation coefficient) are similar to those of biological tissue. The agar-based graphite phantom material is a mixture of water, agar (SCR BR-250G), and graphite powder (LG 100-01) with the mass ratio of 100:3:9. The graphite powder is used to adjust the sound attenuation coefficient. An ultrasound power meter (Ohmic, UPM-DT-1000PA) is employed to precisely control the input ultrasound intensity. In addition, we also experimentally measure the transmittance of the metalens by comparing the output ultrasound intensity with and without the metalens. The result comes to be 68% and it keeps in line with the theoretical value.

To measure the temperature at different locations in the biological phantom, a thermocouple array consisting of six pins (pins a–f) with 2 mm apart is embedded in the phantom cover the focal point. An additional thermocouple pin (pin g) is placed 15 mm away from the focus for monitoring the background temperature, as shown in Figure 3A. The thermocouple array is connected to a thermocouple signal conditioning that recodes the temperature signals. The measured temperature at different positions with the metalens is shown in Figure 3B. At the center of the focal point, a remarkable temperature rise of about 50°C is observed within 10 s, with the input ultrasound power of 4 W. Therefore, the effective ultrasound power after the metalens is 2.72 W. The temperature rise in pin b is measured to be 30°C because it is near the focal region, whereas the temperature rise is much lower in pins c–f whose positions are just 2 mm away

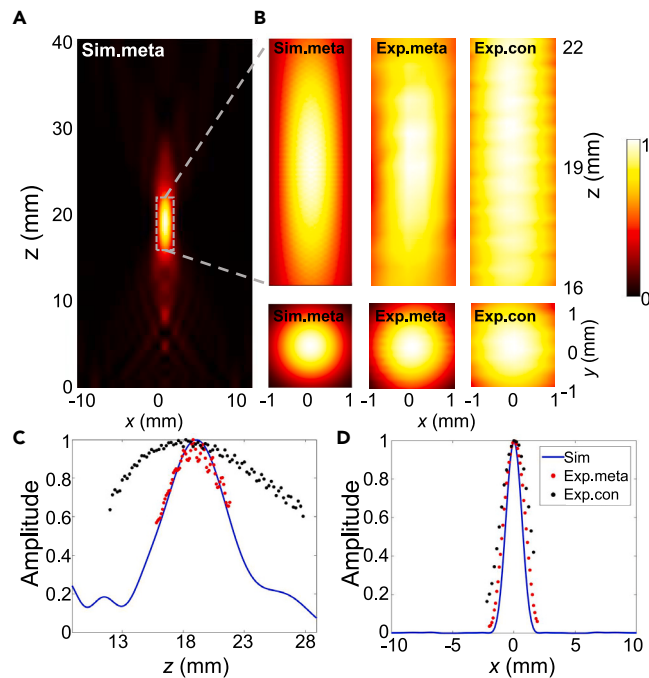


Figure 2. Ultrasound intensity distribution of metalens-based focusing

(A–D) Simulated ultrasound field on x - z plane. Ultrasound intensity distributions on the x - y plane and x - z plane, compared between the simulation and experiments of metalens and concave lens (B). Normalized intensity profiles through the focal spot along (C) the propagation and (D) the transverse directions. Sim.meta, simulation with metalens; Exp.meta, experiment with metalens; Exp.con, experiment with concave lens.

from the focus. On the contrary, the temperature hardly changes in the measurement without the metalens (Figure 3C); it is only 0.5°C within 10 s and increases to 3.7°C after 100 s. The temperature profiles in Figure S1 are plotted in different scales to show a better visualization of the values. Significantly, in order to evaluate the famous "thermocouple artifact effect," we referred to Huang et al. method and measured the temperature rise in an agar-graphite phantom and an agar-only phantom. The results reflect that the temperature remains stable after a brief increase with time in the agar-only phantom, with the stable temperature rise of about 2°C (Figure S2). This effect is relatively insignificant compared with the temperature rise of 50°C observed with the designed metalens, and the overall temperature profile is consistent with the expected focusing performance. Temperature calibration should be conducted if the exact temperature control is required in practical applications.

The infrared thermograph is employed to capture the temperature field map on the focal plane of the metalens and visualize the thermal effect on the biological phantom. The biomedical phantom is placed near on the water-air interface. A block of solid agar of 20 mm thickness and 3% concentration is placed after the metalens, whose acoustic properties are similar to those of water, and a piece of biological phantom of 1 mm thickness is placed on top of the solid agar to make sure that the phantom is located on the focal plane of the metalens. The whole setup is carried out in a water tank. The temperature field maps on the focal plane with and without the metalens are qualitatively captured, as shown in Figure 3D, with the effective input ultrasound power of 2.72 W and at the 10 s radiation time. An obvious focusing profile is observed from the temperature field, where the FWHM agrees with the ultrasound field mapping. A quantitative temperature value inside the biological phantom is inaccessible because the infrared thermograph can only detect the temperature on the surface, where the maximum temperature is measured to be 34°C as a result of the heat conduction in background water.

Thermal effect on in vitro biological specimen

The distinct thermal effect enables the implementation of the metalens as a new ultrasound therapeutic tool to realize the precise and efficient biological tissue ablation, owing to the subwavelength focal resolution and prominent temperature rise at a much lower input energy. Here we use porcine liver as the in vitro biological tissue to demonstrate the tissue ablation effect and investigate the ablation outcomes under different ultrasound parameters. It is convenient to observe the tissue ablation on porcine liver because its hemoglobin will be denatured at about 60°C , making it a good indicator to reveal the thermal effect and study the ablation control by calculating the lesion area and lesion strength on the tissue. In our experiment, a slice of porcine liver tissue of the thickness 1 mm is placed on the focal plane of the metalens. We demonstrate the dependence of the ablation control on the irradiation time and input ultrasound power, as shown in Figure 4. According to the measured temperature profiles at different input ultrasound power shown in Figure 4A, the temperature inside the porcine liver reaches more than 60°C when the input ultrasound power is higher than 3.3 W, and a prompt tissue damage is observed within 3 s at 5.4 W. This input

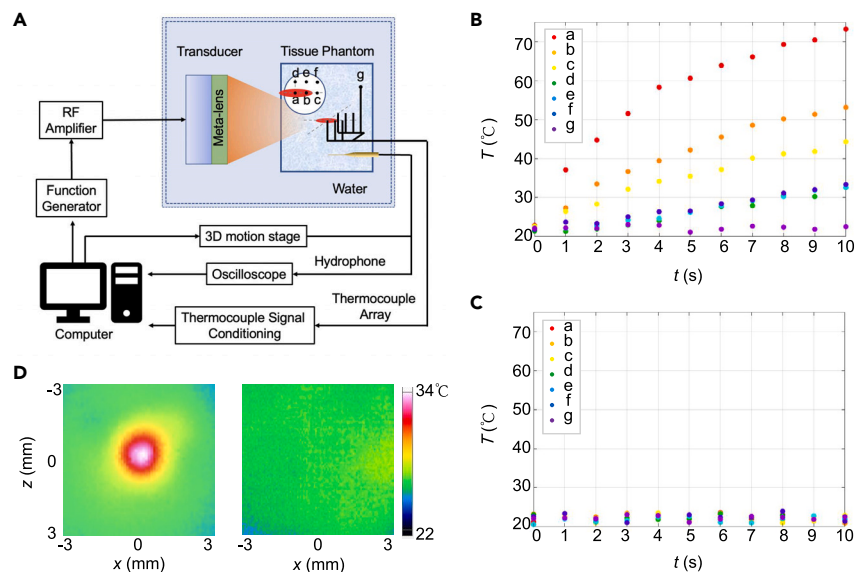


Figure 3. Schematic diagram of the experimental setup for the 3D ultrasound field scanning and temperature monitoring

(A) A hydrophone controlled by a 3D motion stage is used for measuring the ultrasound field after the metalens. A thermocouple array consisting of 6 pins is placed near the focal spot for monitoring the temperature rise. The space between two adjacent thermocouple pins is 2 mm. An additional pin is placed 15 mm away from the focus to measure the background temperature.

(B and C) Temperature profiles recorded by 7 thermocouple pins at different locations, as function of time with (B) and without (C) the metalens.

(D) Experimentally measured infrared thermal imaging of the surface of a biological phantom located at the focal plane for visualizing the temperature field, with (left) and without (right) the metalens.

energy value is much lower than the conventional ultrasound therapeutic method.^{37,38} It can remarkably improve the energy efficiency and safety in the future focused ultrasound treatment. It is noteworthy that the metalens transmittance is 68% in this design. Therefore, the energy efficiency can be further improved by further upgrading the metalens.

The porcine liver tissue after the ultrasound irradiation is imaged with an anatomical microscope. Figure 4B shows the images of the tissue damage with the metalens, with the fixed input ultrasound power of 4 W while under different irradiation time. Obvious lesion is observed on the porcine liver tissue even at 5 s, and the lesion area is increased with the irradiation time. As a comparison, the porcine liver remains intact in the situations without the metalens (Figure 4C). A summary of the images of the porcine liver tissue under the input ultrasound power of 2.6W, 3.3W, 4W, 4.7 W, and 5.4 W, with the fixed irradiation time of 10 s, is shown in Figure 4D. The porcine liver is slightly damaged when the ultrasound power is 2.6 W, and the damage level increases with the input power. To quantitatively assess the ablation effect on biological tissue, we calculate the lesion area and lesion strength. First, the micrographs are binarized to determine the lesion area. Then the integrals of the pixels gray value within the lesion area and the whole image are calculated. The lesion strength is relatively quantified as the ratio between the integrals within the lesion area and whole image. Results are plotted in Figure 4E. The lesion strength is normalized with the maximum damage situation with the input power of 5.4 W. The lesion area gradually increases with the irradiation time, which is about 7.1 mm² at 5 s, and reaches 100.9 mm² at 25 s. When the temperature increases sharply in the high input power situations, the lesion area of porcine liver tissue is also affected by heat diffusion. The experimental results prove that the ablation on the biological tissue induced by the thermal effect of the metalens can be controlled with the irradiation time and input power. In addition, the minimum lesion area of only 7.1 mm² is observed, which is much smaller than results obtained with the phased array method.^{37,38} The small lesion area can contribute to improving the accuracy and safety in the precise ultrasound treatment. It is particularly important in treating the tissue of abundant blood supply or nerve supply, where these blood vessels and neural circuits should be protected from accidental damage during the treatment. Therefore, the high-resolution and high-efficiency ultrasound focusing is expected to have better performance in the precise treatment.

DISCUSSION

In summary, we numerically and experimentally demonstrated an efficient approach of focused ultrasound therapy using a megahertz sub-wavelength metalens. It can induce prominent temperature rise of 50 °C at a much lower input power and controllable ablation effect in biological tissues. The experiment results confirm that the proposed metalens-based ultrasound therapy has prominent advantage of subwavelength resolution, higher positioning precision, energy efficiency, and superior coupling with both the transducer and biological tissue. Benefited from these distinct merits, prompt and obvious tissue ablation on the porcine liver is observed at the input ultrasound power of only 4 W within 5 s, which is much lower than the conventional ultrasound therapeutic method. We also quantitatively assess the lesion

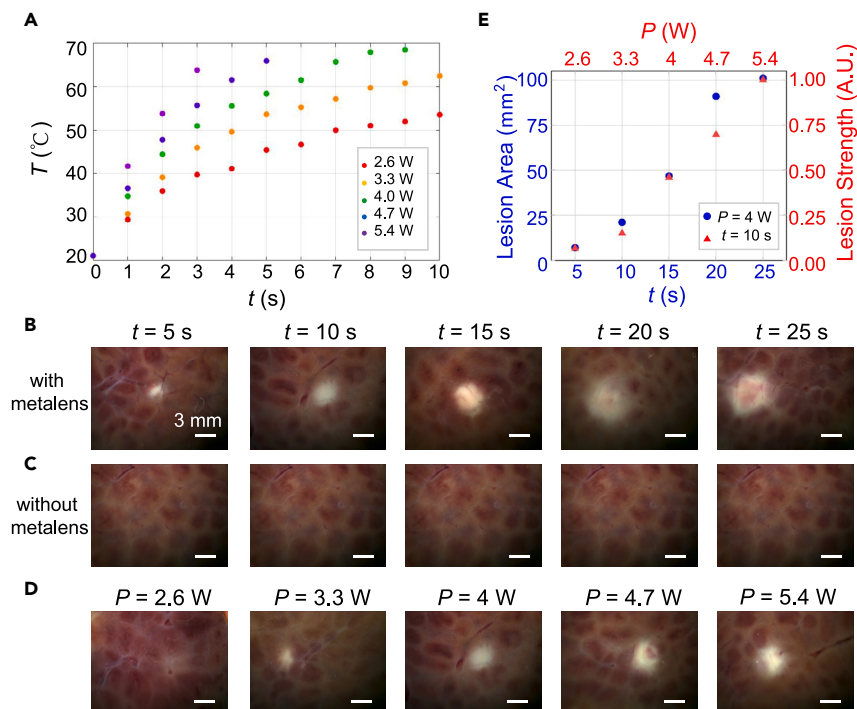


Figure 4. Tissue ablation effect on in vitro biological specimen

(A) Measured temperature at the focal point under different input ultrasound power from 2.6 W to 5.4 W.

(B–E) Summary of the photos of the porcine liver tissue ablation during different radiation time at 4 W (B), and under different input ultrasound power at 10 s (D). Scale bar, 3 mm. (E) The lesion area and lesion strength extracted from (B–D), as functions of the radiation time and input ultrasound power, respectively.

area and lesion strength on the porcine liver, which enables the effective ablation effect control by adjusting the ultrasound parameters. Our work provides a promising strategy to improve the precision, efficiency, and safety in therapeutic ultrasound and facilitate prosperous applications in future clinical trials.

Limitations of study

The most significant limitation is the static focusing performance compared with the active phased array that allows the fast and dynamic beamforming. The development of an active metalens can potentially solve this question by introducing some dynamic control mechanism.

STAR★METHODS

Detailed methods are provided in the online version of this paper and include the following:

- KEY RESOURCES TABLE
- RESOURCE AVAILABILITY
 - Lead contact
 - Materials availability
 - Data and code availability
- METHOD DETAILS
 - Numerical simulations
 - Experimental measurements
 - Biological phantom production
 - Infrared thermography measurements
 - Calculation of lesion area and lesion strength

SUPPLEMENTAL INFORMATION

Supplemental information can be found online at <https://doi.org/10.1016/j.isci.2023.107929>.

ACKNOWLEDGMENTS

This work is supported by the National Natural Science Foundation of China (Grants No. T2222024, 12034005), the National Key R&D Program of China (No. 2022YFA1404500), and the STCSM Science and Technology Innovation Plan of Shanghai Science and Technology Commission (Grant Nos. 20ZR1404200 and 21JC1400300).

AUTHOR CONTRIBUTIONS

Y.Z., X.J., and D.T. developed the concept for the manuscript. Y.Z. designed and performed the experiment, analyzed the data, and prepared the manuscript. C.L. provided advice and support for the thermal effect on the microbiological specifications experimental section. C.Z. and J.J. provided suggestions and support for acoustic simulations and experiments. X.J. and D.T. supervised the study and contributed in the manuscript revision. All authors contributed to this manuscript.

DECLARATION OF INTERESTS

The authors declare no competing interests.

Received: December 16, 2022

Revised: February 21, 2023

Accepted: September 12, 2023

Published: September 16, 2023

REFERENCES

- Madersbacher, S., Kratzik, C., Susani, M., and Marberger, M. (1994). Tissue Ablation in Benign Prostatic Hyperplasia with High Intensity Focused Ultrasound. *J. Urol.* *152*, 1956–1960. , discussion 1960-1. [https://doi.org/10.1016/s0022-5347\(17\)32278-4](https://doi.org/10.1016/s0022-5347(17)32278-4).
- Ward, J.F. (2011). High-intensity focused ultrasound for therapeutic tissue ablation in surgical oncology. *Surg. Oncol. Clin. N. Am.* *20*, 389–407. ix. <https://doi.org/10.1016/j.soc.2010.11.009>.
- Zhou, Y.F. (2011). High intensity focused ultrasound in clinical tumor ablation. *World J. Clin. Oncol.* *2*, 8–27. <https://doi.org/10.5306/wjco.v2.i1.8>.
- Vaezy, S., Martin, R., Schmiedl, U., Caps, M., Taylor, S., Beach, K., Carter, S., Kaczowski, P., Keilman, G., Helton, S., et al. (1997). Liver hemostasis using high-intensity focused ultrasound. *Ultrasound Med. Biol.* *23*, 1413–1420.
- Vaezy, S., Marti, R., Mourad, P., and Crum, L. (1999). Hemostasis using high intensity focused ultrasound. *Eur. J. Ultrasound* *9*, 79–87.
- Noble, M.L., Vaezy, S., Keshavarzi, A., Poun, M., Prokop, A.F., Chi, E.Y., Cornejo, C., Sharar, S.R., Jurkovich, G.J., Martin, R.W., and Crum, L.A. (2002). Spleen hemostasis using high-intensity ultrasound: survival and healing. *J. Trauma* *53*, 1115–1120.
- Martini, S.R., Hill, M.D., Alexandrov, A.V., Molina, C.A., and Kent, T.A. (2006). Outcome in hyperglycemic stroke with ultrasound-augmented thrombolytic therapy. *Neurology* *67*, 700–702.
- Siegel, R.J., and Luo, H. (2008). Ultrasound thrombolysis. *Ultrasonics* *48*, 312–320.
- Behrens, S., Spengos, K., Daffertshofer, M., Schroeck, H., Dempfle, C.E., and Hennerici, M. (2001). Transcranial ultrasound-improved thrombolysis: diagnostic vs. *Ultrasound Med. Biol.* *27*, 1683–1689.
- Wright, C., Hynynen, K., and Goertz, D.J.I.r. (2012). In vitro and in vivo high intensity focused ultrasound thrombolysis. *Invest. Radiol.* *47*, 217.
- Towe, B.C., and Rho, R. (2006). Ultrasonic cardiac pacing in the porcine model. *IEEE Trans. Biomed. Eng.* *53*, 1446–1448.
- Kohut, A.R., Vecchio, C., Adam, D., and Lewin, P.A. (2016). The potential of ultrasound in cardiac pacing and rhythm modulation. *Expert Rev. Med. Devices* *13*, 815–822.
- Ng, K.y., and Liu, Y. (2002). Therapeutic ultrasound: its application in drug delivery. *Med. Res. Rev.* *22*, 204–223.
- Mitragotri, S. (2005). Healing sound: the use of ultrasound in drug delivery and other therapeutic applications. *Nat. Rev. Drug Discov.* *4*, 255–260.
- Yan, F., Li, L., Deng, Z., Jin, Q., Chen, J., Yang, W., Yeh, C.-K., Wu, J., Shandas, R., Liu, X., and Zheng, H. (2013). Paclitaxel-liposome-microbubble complexes as ultrasound-triggered therapeutic drug delivery carriers. *J. Control. Release* *166*, 246–255.
- Tharkar, P., Varanasi, R., Wong, W.S.F., Jin, C.T., and Chrzanowski, W.J.F.i.B. (2019). Nano-enhanced drug delivery and therapeutic ultrasound for cancer treatment and beyond. *Front. Bioeng. Biotechnol.* *7*, 324.
- Oztas, O., Turan, B., Bora, I., Karakaya, M.K., and rehabilitation. (1998). Ultrasound therapy effect in carpal tunnel syndrome. *Arch. Phys. Med. Rehabil.* *79*, 1540–1544.
- Ebenbichler, G.R., Erdogmus, C.B., Resch, K.L., Funovics, M.A., Kainberger, F., Barisani, G., Aringer, M., Nicolakis, P., Wiesinger, G.F., Baghestanian, M., et al. (1999). Ultrasound therapy for calcific tendinitis of the shoulder. *N. Engl. J. Med.* *340*, 1533–1538.
- Busse, J.W., Bhandari, M., Kulkarni, A.V., and Tunks, E. (2002). The effect of low-intensity pulsed ultrasound therapy on time to fracture healing: a meta-analysis. *Can. Med. Assoc. J.* *166*, 437–441.
- Ebbini, E.S., Umemura, S.I., Ibbini, M., Cain, C.A., ferroelectrics, and control, f. (1988). A cylindrical-section ultrasound phased-array applicator for hyperthermia cancer therapy. *IEEE Trans. Ultrason. Ferroelectr. Freq. Control* *35*, 561–572.
- Clement, G.T., White, J., Hynynen, K., and Biology. (2000). Investigation of a large-area phased array for focused ultrasound surgery through the skull. *Phys. Med. Biol.* *45*, 1071–1083.
- Wu, X., Sherar, M., and Biology. (2002). Theoretical evaluation of moderately focused spherical transducers and multi-focus acoustic lens/transducer systems for ultrasound thermal therapy. *Phys. Med. Biol.* *47*, 1603–1621.
- Li, F., Wang, H., Zeng, D., Fan, T., Geng, H., Tu, J., Guo, X., Gong, X., Zhao, C., Wang, Z., et al. (2013). Sub-wavelength ultrasonic therapy using a spherical cavity transducer with open ends. *Appl. Phys. Lett.* *102*, 204102.
- Chen, D.-C., Zhu, X.-F., Wei, Q., Wu, D.-J., and Liu, X.J. (2018). Broadband acoustic focusing by Airy-like beams based on acoustic metasurfaces. *J. Appl. Phys.* *123*, 044503.
- Hur, S., Choi, H., Yoon, G.H., Kim, N.W., Lee, D.-G., and Kim, Y.T. (2022). Planar ultrasonic transducer based on a metasurface piezoelectric ring array for subwavelength acoustic focusing in water. *Sci. Rep.* *12*, 1485–1511.
- Cummer, S.A., Christensen, J., and Alù, A.J.N.R.M. (2016). Controlling sound with acoustic metamaterials. *Nature* *536*, 1–13.
- Tang, K., Qiu, C., Lu, J., Ke, M., and Liu, Z. (2015). Focusing and directional beaming effects of airborne sound through a planar lens with zigzag slits. *J. Appl. Phys.* *117*, 024503.
- Chen, J., Rao, J., Lisevych, D., and Fan, Z. (2019). Broadband ultrasonic focusing in water with an ultra-compact metasurface lens. *Appl. Phys. Lett.* *114*, 104101.
- Calvo, D.C., Thangawng, A.L., Nicholas, M., and Layman, C.N. (2015). Thin Fresnel zone plate lenses for focusing underwater sound. *Appl. Phys. Lett.* *107*, 014103.
- Walker, E.L., Jin, Y., Reyes, D., and Neogi, A. (2020). Sub-wavelength lateral detection of tissue-approximating masses using an ultrasonic metamaterial lens. *Nat. Commun.* *11*, 5967–6013.

31. Jiang, X., He, J., Zhang, C., Zhao, H., Wang, W., Ta, D., and Qiu, C.-W. (2022). Three-dimensional ultrasound subwavelength arbitrary focusing with broadband sparse metalens. *Sci. China Phys. Mech.* *65*, 1–7.
32. He, J., Jiang, X., Zhao, H., Zhang, C., Zheng, Y., Liu, C., and Ta, D.J.P.R.A. (2021). Broadband Three-Dimensional Focusing for an Ultrasound Scalpel at Megahertz Frequencies. *Phys. Rev. Applied* *16*, 024006.
33. Zhu, H., Zhou, K., Zhang, L., Jin, C., Peng, S., Yang, W., Li, K., Su, H., Chen, W., Bai, J., et al. (2009). High intensity focused ultrasound (HIFU) therapy for local treatment of hepatocellular carcinoma: role of partial rib resection. *Eur. J. Radiol.* *72*, 160–166.
34. Zhang, L., Zhu, H., Jin, C., Zhou, K., Li, K., Su, H., Chen, W., Bai, J., and Wang, Z. (2009). High-intensity focused ultrasound (HIFU): effective and safe therapy for hepatocellular carcinoma adjacent to major hepatic veins. *Eur. Radiol.* *19*, 437–445.
35. Jang, H.J., Lee, J.-Y., Lee, D.-H., Kim, W.-H., Hwang, J.H.J.G., and liver. (2010). Current and future clinical applications of high-intensity focused ultrasound (HIFU) for pancreatic cancer. *Gut Liver* *4*, S57.
36. Burlew, M.M., Madsen, E.L., Zagzebski, J.A., Banjavic, R.A., and Sum, S.W. (1980). A new ultrasound tissue-equivalent material. *Radiology* *134*, 517–520.
37. Bobkova, S., Gavrilov, L., Khokhlova, V., Shaw, A., Hand, J., and biology. (2010). Focusing of high-intensity ultrasound through the rib cage using a therapeutic random phased array. *Ultrasound Med. Biol.* *36*, 888–906.
38. Yuldashev, P.V., Shmeleva, S.M., Ilyin, S.A., Sapozhnikov, O.A., Gavrilov, L.R., and Khokhlova, V.A.; Biology (2013). The role of acoustic nonlinearity in tissue heating behind a rib cage using a high-intensity focused ultrasound phased array. *Phys. Med. Biol.* *58*, 2537–2559.

STAR★METHODS

KEY RESOURCES TABLE

REAGENT or RESOURCE	SOURCE	IDENTIFIER
Software and algorithms		
MATLAB	MathWorks	https://www.mathworks.com/products/matlab.html
COMSOL MULTIPHYSICS	COMSOL	http://cn.comsol.com/

RESOURCE AVAILABILITY

Lead contact

Further information and requests for resources and reagents should be directed to and will be fulfilled by the lead contact, Xue Jiang (xuejiang@fudan.edu.cn).

Materials availability

This study did not generate new unique reagents.

Data and code availability

- All data reported in this paper will be shared by the [lead contact](#) upon request.
- This paper does not report original code.
- Any additional information required to reanalyze the data reported in this paper is available from the [lead contact](#) upon request.

METHOD DETAILS

Numerical simulations

The numerical simulations are conducted based on COMSOL MULTIPHYSICS software in Acoustics Module, Frequency Domain. A schematic plot of the simulation setup is shown in [Figure S3](#). The incident ultrasound wave is generated by the plane wave radiation boundary and propagates from the bottom. Three cylindrical perfectly matched layers (PML) are used in the simulation to avoid the reflection and mimic the propagation in free space. The metalens in simulation is made of resin and silicone. To accurately resolve pressure gradient abrupt changes in the focus region, the model uses a refinement grid of size $\lambda/8$ ($\lambda = 1.5$ mm is the wavelength). Ultrasound pressure is discretized using the default secondary (second-order) unit. Since the transducer is a circular planar transducer arranged coaxially with the circular metalens, the simulation can be simplified as a two-dimensional axisymmetric model to save the computation time.

Experimental measurements

The experimental measurements are conducted in a 3D water tank with its dimensions of 500 mm, 500 mm and 500 mm respectively. We fabricate a sample of the resin-silicone metalens and a concave lens which has same focal length using three-dimensional (3D) printing and pouring molding technologies. In the first step, the resin plate consisted of different annular grooves is 3D printed. In the second step, the liquid silicone gel (Posilicon DRSGJ02) is injected into the grooves which will curd after 6–8 h. The schematic diagram of the experimental setup for the ultrasound field scanning and the temperature monitoring is depicted in [Figure 3A](#). The monochromatic signal generated by the function generator (Keysight, 33500B Series) and amplified by the power amplifier (Aigtek, ATA-2021H) is fed into a flat ultrasound transducer (Olympus, center frequency 1 MHz, radius 25 mm, effective vibration surface radius 21 mm) which emits the plane ultrasound wave propagating along z direction. The metalens is tightly attached to the transducer by ultrasound coupling agent (Hynaut 56201). In the ultrasound field scanning, a needle hydrophone (Precision Acoustics, NH0500) controlled by the 3D motion stage is used to receive the ultrasound. Its signal is collected by an oscilloscope (Keysight, DSOX4024A) and post-processed using MATLAB R2020a software. The field scanning is carried out in the x-y plane (2 mm × 2 mm) and x-z plane (2 mm × 6 mm) with the scanning step of 100 μ m.

Biological phantom production

Heated the water to 90°C and then added agar and graphite powder successively. Stir at this temperature quickly until uniform. To prevent sedimentation of graphite powder, rapid solidification of agar-based graphite phantom material is required. In the study, uniform mixture is placed in a refrigerator at -4°C so that the mixture will be solidified within 2 h (depending on the total volume). Mixture placed at indoor temperature will be solidified within 6 h but will result with uneven graphite powder distribution in the phantom.

Infrared thermography measurements

The infrared thermal imager can accurately capture the temperature profile on the object surface. Therefore, we place the biomedical phantom on the water-air interface, as schematically shown in [Figure S4](#). Specifically, an agar block of 20 mm thickness (same as the focal length) and 3% concentration is placed on the metalens, and a piece of biomedical phantom of 1 mm thickness is placed on top of the agar block to make sure that it is on the focal plane. An infrared thermal imager is vertically located above the biomedical phantom and images the thermal map on the focal plane. The vertical setup also helps to avoid the light reflection from walls of the water tank.

Calculation of lesion area and lesion strength

First, the micrographs are binarized to determine the lesion area. Then the integrals of the pixels gray value within the lesion area and the whole image are calculated. The lesion strength is relatively quantified as the ratio between the integrals within the lesion area and whole image.